Volume 1 | Number 1 | Jan 2013 | Pages 1–100

Journal of
**Materials Chemistry A**

Materials for energy and sustainability
www.rsc.org/materialsA

Li⁺

ROYAL SOCIETY
OF CHEMISTRY

ROYAL SOCIETY
OF CHEMISTRY

www.rsc.org/materialsA

Graphical abstract of

"**Colloidal Au Single-Atom Catalysts Embedded on Pd Nanocluster**" **authored by** Haijun

Zhang, Keisuke Kawashima, Mitsutaka Okumura, and Naoki Toshima

**Activity:**



◯ : Pd atom    🔴 : Au atom
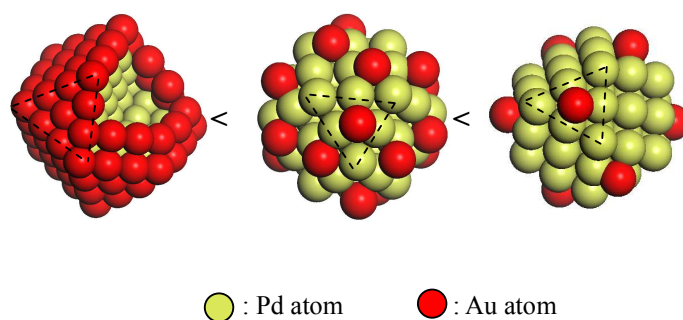
The activity for glucose oxidation of colloidal Au/Pd single-atom catalysts was 17 times higher than

Au NCs with similar sizes.

# Colloidal Au Single-Atom Catalysts Embedded on Pd Nanocluster

Haijun Zhang[1]*, Keisuke Kawashima[2], Mitsutaka Okumura[3], and Naoki Toshima[2]*

[1.] *The State Key Laboratory of Refractories and Metallurgy, Wuhan University of Science and Technology, Wuhan, Hubei Province 430081, China*

[2.] *Department of Applied Chemistry, Tokyo University of Science Yamaguchi, SanyoOnoda, Yamaguchi 756-0884, Japan*

[3.] *Graduate School of Science, Osaka University, Machikaneyama, Toyonaka, Osaka 560-0043, Japan*

*Corresponding author, E-mail: toshima@rs.tus.ac.jp; zhanghaijun@wust.edu.cn

**Abstract**

This work aims to design an efficient Au single-atom catalyst (SAC) for aerobic glucose oxidation and obtain a clear structure-activity relationship of the catalyst at the atomic level. Gold-containing bi- or multi-metallic catalysts are widely used in many important chemical processes. Engineering the electronic structure of surface atoms and downsizing the catalysts to single atoms are challengeable issues to enhance the intrinsic activity. Here we report an effective and versatile synthesis of colloidal Au/Pd SACs by using a facile successive reduction method. The prepared colloidal Au/Pd SACs exhibit a significantly improved catalytic activity (up to 17 times) for glucose oxidation over that of Au nanoclusters (NCs) with a similar size. High-angle annular dark-field scanning transmission electron microscopy (HAADF-STEM) analysis and density functional theory (DFT) calculation reveal that the presence of the low-coordinated and negatively charged single Au atoms on Pd clusters is responsible for the excellent catalytic performance.

**Keywords**: Single-atom catalyst; Au; Catalytic activity; Au/Pd; Cluster; Colloidal catalysts; Glucose oxidation

## 1. INTRODUCTION

Catalysts play crucial roles in many chemical and energy conversion processes. Precious metals and rare metals are often the major components of active catalysts. Many efforts have been made to maximize the utilization of these metals [1-8]. The research into downsizing the metal particles to nanoparticles, nanoclusters (NCs) and atoms, therefore, attracts much attention during recent several years [1-10]. As the size of metal nanostructures is decreased from nanometer to subnanometer scale and ultimately to single atoms, the catalytic performance may change significantly due to the low-coordination environment, quantum size effect, and improved metal-support interactions. [11].

The ultimate small-size limit for the precious and rare metal particles is the single-atom catalyst (SAC), which contains isolated metal atoms singly dispersed on supports [11]. Single-atom catalysis is of increasing interest as a novel branch of heterogeneous catalysis due to the high activity and/or selectivity for numerous important catalytic reactions with low cost [12-20]. Zhang's group [14-15] reported that a $Pt_1/FeO_x$ SAC shows both excellent stability and high activity for CO oxidation, and preferential oxidation of CO in the presence of $H_2$. It is proposed that the high activity of the $Pt_1/FeO_x$ SAC correlates with the presence of high-valence Pt atoms (with partially vacant $5d$ orbital and a slightly positive charge), which help to reduce both the CO adsorption energy and activation energy barriers for CO oxidation. In addition, the activity of $Ir/Fe(OH)_x$ SAC for preferential oxidation of CO was also reported by the same group [16]. The activity of the $Ir/Fe(OH)_x$ SAC is at least one order of magnitude higher than traditional Ir-based catalysts. Szanyi *et. al* [17] reported on the very unique catalytic properties of isolated Pd atoms for the reduction of $CO_2$. The results showed that atomically dispersed supported metals can be catalytically active even

in the demanding reaction of $CO_2$ reduction. Heiz and co-workers' experimental work [18-19] established beyond doubt that a single metal atom of palladium, supported on magnesia (MgO) facilitates the cyclotrimerization of acetylene [18] and the oxidation of CO by $O_2$ to $CO_2$ [19]. More recently, Sun *et al.* [20] reported a systematic study in which atomic layer deposition was used to synthesize platinum SAC deposited on the surface of graphene nanosheets. The prepared Pt SACs exhibit significantly improved catalytic activity (up to 10 times) over that of the state-of-the-art commercial Pt/C catalyst. The less-coordinated and unsaturated 5d orbitals of the single Pt atoms are responsible for the excellent electrochemical performance. Kyriakou *et al.* [22] reported that individual, isolated Pd atoms dispersed onto Cu surfaces dissociated hydrogen and facilitated the spillover of H, resulting in selective hydrogenation of styrene and acetylene. Even the supported SACs are unique and indeed bridge the gap between homogeneous and heterogeneous catalysis. However, the large-scale synthesis of SACs remains a significant challenge because single atoms are too mobile and easy to sinter under realistic reaction conditions [23]. Up to date, almost all of the SACs reported so far are limited to single metal atoms anchored to solid supports (metal oxides, graphene nanosheets, carbon, metal surfaces, metal-organic frameworks and zeolites) [12-24]. It should be emphasized that the annealing process of the supported catalysts will doubtlessly result in the growth and aggregation of the prepared single metal atoms.

There are several major advantages of colloidal catalysts compared with the supported ones [25]. For example, 1) the intrinsic properties of metal colloidal catalysts can be relatively easily elucidated without the effect of the metal-support interaction, 2) the NCs with more uniform particle sizes can be obtained in the dispersed systems than in the supported cases, especially under conditions at a high metal concentration, and 3) high stability can be easily got for the colloidal catalysts due to good protection of active sites by a protective agent. Colloidal SACs also exhibit

excellent catalytic activity. Our group [26-27] prepared Crown Jewel-structured Au/Pd SACs by a galvanic replacement reaction method, where gold atoms were atomically dispersed on the top sites of Pd nanoclusters, and the as-prepared colloidal Au/Pd SACs showed unprecedentedly high activity for glucose oxidation. Nevertheless, it should be noted that the applicability of the galvanic replacement reaction for preparation of colloidal SACs is still limited, and that the method can only lead to the deposition of more noble element and dissolution of the less noble component. Moreover, the reaction process of galvanic replacement is somewhat complex and the final structure of the prepared catalysts is highly dependent on the shape and size of the mother cluster and the kind of protective reagent [27-28].

Au/Pd bimetallic nano-catalysts are one of the most interesting systems in catalysis research. The catalysts have been studied for a number of reactions: direct synthesis of hydrogen peroxide from $H_2$ and $O_2$ [29-30], oxidation of alcohols to aldehydes [31], CO oxidation [32], gas-phase hydrodehalogenation of fluorinated compounds [33], hydrogenation of 4-pentenoic acid [34], and hydrodesulfurization of thiophenes [35]. We demonstrate here that an effective and versatile tool to prepare colloidal Au/Pd SACs by a facile successive reduction method using *L*-ascrobic acid as reducing reagent on a large scale. Characterization, catalytic activities for aerobic glucose oxidation and DFT (Density Functional Theory) calculations of the colloidal SACs, and, in addition, the correlations between the geometric/electronic structures of the single Au atoms and the catalytic activity of the SACs were investigated. The studies demonstrated that the activity of the single Au atoms for aerobic glucose oxidation is closely dependent on its geometric structures and its negative charge density. These findings could be exploited to develop more efficient Au-containing bi- or multi-metallic nanostructures by design and have also broad implications for making the most efficient use of other precious metals in many and various electro- and/or thermal-catalytic

technologies.

## 2. EXPERIMENTAL SECTION

### Materials

Hydrogen tetrachloroaurate(III) tetrahydrate (HAuCl$_4$·4H$_2$O, 99.9%) purchased from Tokyo Kasei Kogyo, Ltd., and palladium chloride (PdCl$_2$, 99.9%) and PVP (poly(*N*-vinyl-2-pyrrolidone, K35, molecular weight about 40,000) both purchased from Wako Pure Chemical Industries, Ltd., were used without further purification. All glassware and Teflon-coated magnetic stirring bars were cleaned with aqua regia, followed by copious rinsing with purified water. The water was purified by a Millipore Milli-RX 12 plus water system.

### Preparation of PVP-Protected Pd NCs (Mother Clusters)

Preparation of the dispersions of the PVP-protected Pd NCs was carried out by an alcohol reduction method [36]. A solution of PdCl$_2$ (50 mL, 0.66 mM, ethanol/water=1/4, v/v) was added to a PVP solution (50 mL, 66 mM, ethanol/water=1/4, v/v) and then stirred at room temperature for 15 min. The mixed solutions were stirred and heated to refluxing at 90°C for 0.25, 0.5, and 1 h, and the corresponding Pd mother NCs prepared were designated as Pd(0.25h), Pd(0.5h), and Pd(1h), respectively. The color of the mixed solutions slowly changed from dark yellow to a transparent brown at the beginning of the refluxing. The colloidal dispersions were filtered by an ultrafilter membrane with a cutoff molecular-weight of 10,000 (Toyo Roshi Kaisha, Ltd.) and washed twice with water and then once with ethanol under nitrogen to remove any extra reagents and byproducts. The residual ethanol in the PVP-protected Pd NCs was removed by using a rotary evaporator at 40°C.

UV-Vis spectra, TEM image and size distribution histogram of the PVP-protected Pd mother

NCs are shown in Figures S1-S2, respectively. The average sizes (± standard deviation) based on the TEM images (Figure S2) are 1.7 ± 0.3 nm for Pd(1h) NCs, 1.5 ± 0.4 nm for Pd(0.5h) NCs, and 1.4 ± 0.5 nm for Pd(0.25h) NCs, respectively. In the case of the Pd(0.25h) NCs mother clusters, the population of the PVP-protected Pd NCs has a peak at a diameter of about 1.4 nm, indicating that the Pd mother NCs consist of about 55 atoms in a particle on the average. We characterize this as the size-selected $Pd_N$ (where N=55) NCs, where $Pd_{55}$ is known to be a possible 'magic number' cluster [37]. The $Pd_{55}$ NC with the ideal size of about 1.4 nm can be characterized as a truncated octahedron with eight triangular {111} faces and six square {100} faces (Figure 1). The mean particle diameters were used for the approximate calculation and preparation of the PVP-protected colloidal Au/Pd SACs in the following steps. Here, we simply consider that all the prepared 'Pd mother clusters' possess the ideal structure of $Pd_{55}$, and that the defect sites including kink atoms, twinning boundaries, and stacking faults are not taken into consideration.

### Preparation of Colloidal Au/Pd SACs

The colloidal Au/Pd SACs were prepared by a successive reduction method which is usually used to prepare core/shell-structured NCs using $L$-ascrobic acid ($C_6H_8O_6$) as reducing reagent (as shown in Figure 1). For example, the SA-6 colloidal SACs (the atomic ratio of $Au^{3+}$ to Pd in the synthetic solution = 3/55) were prepared as follows: Aqueous solutions of $HAuCl_4 \cdot 4H_2O$ (15 mL, 0.048 mM) and PVP (15 mL, 4.8 mM) were mixed together for 0.5 h at room temperature at first, and then the mixed solutions were rapidly added to an as-prepared PVP-protected colloidal dispersion of Pd mother clusters (Pd(0.25h), 30 mL, 0.44 mM) containing $L$-ascrobic acid (0.0144 mmol) under condition of continuous stirring at room temperature in an $N_2$ atmosphere. The mixtures were then further treated by heat for 0.25 h in a bath at 95°C. The transparent and brownish dispersions were then obtained. The colloidal dispersions of Au/Pd SACs were purified and concentrated by washing

and rotary evaporating. The PVP-protected Au/Pd SACs were finally obtained as powders by vacuum drying at 40°C for 48 h.

In order to get the best conditions for preparing the SACs, the kinds of Pd mother clusters of Au/Pd were varied as parameters, and three kinds of colloidal Au/Pd SACs were prepared and then used as colloidal catalysts for the aerobic oxidation of glucose. (Preparation conditions varied with kinds of mother cluster and composition of Au/Pd are shown in Table S1.) The UV-Vis absorption spectra, TEM micrographs and size distribution histograms of as-prepared three kinds of $Au_{55}Pd_{55}$ catalysts are shown in Figures S3-S4, respectively. The average sizes ($\pm$ standard deviation) of $Au_{55}Pd_{55}$ catalysts prepared by using Pd(0.25h), Pd(0.5h), and Pd(1h) NCs as mother clusters were estimated to be $1.8 \pm 0.5$ nm, $1.8 \pm 0.9$ nm, and $2.0 \pm 0.9$ nm, respectively. Comparing Figures S3-S4 with Figures S1-S2 can give the following findings: 1) Au is deposited on the surface of Pd mother NCs. 2) It is suggested that large Pd mother NCs (Pd(1h)) can catch a larger amount of Au atoms than the small one, which form larger Au clusters on the surface of Pd NC. The chemical compositions of the $Au_{55}Pd_{55}$ catalysts were obtained from the ICP analysis as shown in Table S2. Comparison of the Au atomic% in the final catalysts and that in the metal precursor feed indicates that the atomic ratio of Au in the feed in the synthetic solution was approximately equal to that in the final catalysts. The catalytic activity for the aerobic oxidation of glucose of the as-prepared three kinds of $Au_{55}Pd_{55}$ catalysts increased in the order $Au_{55}Pd(1h)_{55} < Au_{55}Pd(0.5h)_{55} \approx Au_{55}Pd(0.25h)_{55}$ (Figure S5). The highest catalytic activity of about 17,200 mol-glucose·h$^{-1}$·mol-Au$^{-1}$ was achieved for the smallest $Au_{55}Pd_{55}$ catalysts prepared using Pd(0.5h) and Pd(0.25h) NCs as mother clusters.

**Characterization of NCs**

The UV−Vis (ultraviolet and visible light) absorption spectra were measured over the range of 200-800 nm by a Shimadzu UV-2500PC recording spectrophotometer using a quartz cell with a

10-mm optical path length.

Transmission electron microscopy (TEM) images were obtained using a JEOL TEM 1230 at the accelerated voltage of 80 kV. The specimens were obtained by placing one or two drops of the colloidal ethanol solution of the Au/Pd SACs onto a thin amorphous carbon film-covered copper microgrid and drying it in air at room temperature. Prior to the specimen preparation, the colloidal ethanol solutions were sonicated for 10 min to obtain a better particle dispersion on the copper grid. Image analysis was performed using iTEM software (Olympus Soft Imaging Solution GmbH). For each sample, generally at least 200 particles from different parts of the grid were used to estimate the mean diameter and size distribution of the particles.

Dark field scanning transmission electron microscopy (DF-STEM) was observed with a JEOL TEM 2010F microscopy at accelerated voltage of 200 kV at UBE Scientific Analysis Laboratory, Japan. Energy dispersion X-ray spectroscopy (EDS) measurements were carried out with a NORAN UTW type Si(Li) semiconducting detector with about 1 nm beam diameter attached to the STEM equipment.

The high-angle annular dark-field scanning TEM (HAADF-STEM) were observed using a JEOL TEM 2010F microscope equipped with CEOS spherical aberration correctors at the accelerating voltage of 120 kV in the UBE Scientific Analysis Laboratory, Japan. High-resolution electron energy loss spectroscopy (EELS) measurements were carried out using an ENFINA1000 detector (Gatan, Inc.) with about a 0.15 nm beam diameter attached to the HAADF-STEM equipment.

The metal content of the colloidal Au/Pd SACs was determined by optical emission spectroscopy with inductive coupled plasma (ICP-OES, Varian 720-ES). For this purpose, 2-3 mg of the samples were solubilized in 2 mL of aqua regia ($HCl/HNO_3=3/1$, vol) for 24 h, and then the solubilized solution was diluted to 20 mL by using pure water for the measurement.

**Catalytic Properties**

The catalytic performance of all the catalysts was evaluated using the glucose oxidation as a model reaction. The reactions were carried out at 60°C in a 50-mL glass beaker placed in a thermostat (about 2000 mL). During the experiment, the pH of the reaction suspension was kept constant at 9.5 by the addition of a 1 mol L$^{-1}$ NaOH solution using an automatic potentiometric titrator (Kyoto Electronics MFg., Co., Ltd., Japan). Oxygen was bubbled through the suspension at the flow rate of 100 mL min$^{-1}$ and at atmospheric pressure. The suspension was vigorously stirred by a magnetic stirrer. The starting concentration and volume of the glucose solution was 0.264 mol L$^{-1}$ and 30 mL, respectively, and the charged weight of the catalyst was about 2 mg. The catalytic reactions were automatically carried out for 2 h. The activity (mol-glucose·h$^{-1}$·mol-M$^{-1}$) was calculated from the slope of a straight line fitted using the NaOH amount vs reaction time curve. The initial specific activity related to the metal content of the catalysts was calculated for comparison. A typical NaOH amount vs time diagram with the fit line is shown in Figure S6. The slope of the fit line reflects the initial activity of the catalyst. The catalytic activities of all the samples were measured at least twice under the same conditions and the mean value of the measuring results was used as for comparison.

The activities of the single Au atoms were approximately calculated by subtracting the catalytic activity of Pd atoms in the $Au_{20}Pd_{80}$ alloy nanoclusters from that of AuPd SACs by using the following equation 1:

$$G_{Pd,atom} \times X_{Pd} + G_{Au,atom} \times X_{Au} = G_{Au/Pd} \tag{1}$$

where $G_{Au/Pd}$ are the catalytic activities of the PVP-protected Au/Pd SACs, which were evaluated by the above-mentioned method. $X_{Pd}$ and $X_{Au}$ are the atomic ratios of Pd and Au in the colloidal Au/Pd SACs, respectively, which were measured by ICP-OES. $G_{Au, atom}$ is the calculated catalytic activity

of the Au atoms in the prepared Au/Pd SACs. To eliminate the alloying effects upon the Pd atoms, the normalized catalytic activity $G_{Pd, atom}$ (mol-glucose·h$^{-1}$·mol-Pd$^{-1}$) of the Pd atoms in Au$_{20}$Pd$_{80}$ alloy NCs but not the activity of pure Pd mother NCs (The activity for glucose oxidation of the Pd(0.25h) mother clusters is very low with a value of about 2,670 mol-glucose·h$^{-1}$·mol-Pd$^{-1}$.) was used for the calculation. Thus, the $G_{Pd, atom}$ with a value of about 5,000 mol-glucose·h$^{-1}$·mol-Pd$^{-1}$ was approximately estimated by the following relationship; $G_{Pd, atom}$ (in alloy) = $(G_{Au20Pd80}-0.2G_{Au,NCs})/0.8$, where $G_{Au20Pd80}$ (5,250 mol-glucose·h$^{-1}$·mol-M$^{-1}$) and $G_{Au, NCs}$ (6,230 mol-glucose·h$^{-1}$·mol-Au$^{-1}$) are the catalytic activities for glucose oxidation of Au$_{20}$Pd$_{80}$ alloy NCs and pure Au NCs prepared by rapid injection of NaBH$_4$, respectively. The average particle sizes of the Au$_{20}$Pd$_{80}$ alloy NCs and pure Au NCs were 2.4 ± 0.8 and 1.4 ± 0.5 nm, respectively.

**Density Functional Theory (DFT) Calculation**

The structure and properties of the M$_{55}$ clusters are calculated using the DMol$^3$ DFT package. In these calculations, an all-electron relativistic core treatment and a doubled numerical basis set with polarization functions were employed. The rPBE functional is used for the DFT calculations. For all calculations, the spin restricted SCF calculations were carried out with a convergence criterion of 10$^{-5}$ a.u. for the total energy and the electron density. We used the convergence criteria of 0.004 hartree/A on the force parameters, 0.005 A on the displacement parameter, and 2×10$^{-5}$ hartreee on the total energy in the geometry optimization. The Hirshfeld population analysis was used for the investigation of the atomic charges of the investigated clusters. For these calculations, DNP basis sets are used for the atoms in the model systems.

## 3. RESULTS AND DISCUSSION

### 3.1 Preparation of Colloidal Au/Pd SACs

Successive reduction involves the reduction of the first metal ions, followed by the reduction of the second metal ions. The second metals are usually deposited on the surface of the first metals due to the formation of the strong metallic bond, resulting in core/shell-structured BNPs. By using this strategy, core/shell-structured BNPs with Au as a shell can be easily prepared [38-45]. We tried to prepare colloidal Au/Pd SACs by a successive reduction method using *L*-ascrobic acid as a reducing reagent. Herein, *L*-ascrobic acid acts as the suitable reducing agent to ensure the deposition of Au atoms on the surface of Pd mother clusters due to its weak reduction ability, and then further promote the formation of the Au/Pd SACs, rather than individual monometallic Pd and Au NCs. In order to avoid the occurrence of galvanic replacement between $Au^{3+}$ and Pd mother clusters as much as possible, heat treatment to reaction temperature was carried out as quick as possible after *L*-ascrobic acid, Pd mother cluster dispersions and $Au^{3+}$ ion solutions were mixed together. The standard reduction potentials (SRPs) (relative to the standard hydrogen potential, $H^+/H^0 = 0.00V$) of $C_6H_8O_6/C_6H_6O_6$ and $Pd^{2+}/Pd^0$ are -0.06 V and 0.951 V, respectively, both of which are lower than that of $Au^{3+}/Au^0$ (1.498 V). The reducing ability of *L*-ascrobic acid is much stronger than that of Pd mother clusters. Thus, it is reasonably estimated that most of the $Au^{3+}$ ions would react with *L*-ascrobic acid first and then in-situ reduced on the surface of the mother clusters. The relative standard deviations in the sizes of produced Au/Pd SACs are at the same level of those of mother clusters, as mentioned later. This fact also supports the present idea that the produced Au atoms are deposited on the surface of the Pd mother clusters.

A series of colloidal Au/Pd SACs with various Au contents were prepared to investigate the relationship between Au contents and catalytic activity of SACs based on the previously mentioned best conditions for Au depositions using Pd(0.25h) NCs as mother clusters. The details of compositions and preparation conditions are shown in Table S3. Colloidal dispersions of Au/Pd

SACs with Au contents varying from 5.2 to 62.6 atomic % (theoretical content) were obtained by reduction of the corresponding $Au^{3+}$ ions with *L*-ascrobic acid under nitrogen atmosphere. The resulting colloidal catalysts are homogeneous, dark-brown in color, and stable for months without precipitation. The UV-Vis absorption spectra of the aqueous dispersions of $Pd_{55}$ mother clusters and a series of Au/Pd SACs with various contents of Au are shown in Figure 2. The peak around 290 nm in the curves of Figure 2 was caused by the presence of *L*-ascrobic acid since the samples for UV-Vis measurement were original solutions without membrane filtration. Moreover, the results show that the absorbance intensities of UV-Vis spectra of the Au/Pd SACs are higher in the entire measuring range than those of the $Pd_{55}$ mother NCs (Figure 2) though the concentrations of the Au/Pd SAC dispersions are almost same with that of $Pd_{55}$ mother NCs. The absorbance intensity increases with the increasing Au content, and the absence of the surface plasmon peak of Au at 520 nm for SA-1, SA-2, SA-3, SA-4, and SA-5 NCs indicates that Au atoms are deposited only in several areas across the surface of the $Pd_{55}$ NCs. However, a rather strong plasmon peak at 550 nm was observed for the SA-6 NCs ($Au_{55}Pd_{92}$), suggesting the formation of a core/shell structure with Pd as a core and Au as a shell, where isolated Au clusters could be located on the surface of the Pd NCs.

Figure 3 shows a representative set of TEM images (size distribution histograms are shown in Figure S7) of the colloidal Au/Pd SACs. All the clusters are spherical and well-isolated, mainly distributed within the range from about 0.75 to 4 nm. The average sizes (± standard deviation) based on the TEM images are 1.5 ± 0.5 nm for SA-1, 1.5 ± 0.4 nm for SA-2, 1.6 ± 0.5 nm for SA-3, 1.7 ± 0.5 nm for SA-4, 1.8 ± 0.5 nm for SA-5, and 2.6 ± 1.5 nm for SA-6. All the average particle sizes of the colloidal Au/Pd SACs are larger than the Pd mother NCs (1.4 nm) and increase with increasing the $Au^{3+}$ ion contents fed. This is well consistent with the results of UV-Vis in Figure 2.

Moreover, these results provide additional evidence that Au atoms are indeed deposited on the surface of the Pd mother NCs. These results are also supported by the ICP analysis of the prepared Au/Pd SACs. The chemical compositions of the SACs, obtained by the ICP analysis and shown in Figure 4 and Table S4, indicate that the atomic Au ratio of the feed in the synthetic solution is approximately equal to the resulting Au atomic ratio in the final Au/Pd SACs. Thus, it could be reasonably suggested that all the $Au^{3+}$ ions in the synthetic solution were reduced to Au.

### 3.2 Structure Characterization and Catalytic Activity of the Colloidal Au/Pd SACs

Scanning transmission electron microscopy (STEM) in conjunction with atomic-scale EDS could provide insight into the change of surface composition [46–48]. We demonstrate that the Au atoms can be deposited on the surface of Pd mother NCs. To obtain detailed information about the morphology and the particle size of the synthesized sample, STEM-EDS was carried out firstly. Figure 5 represents the STEM (a) and STEM-EDS (b) images of $Au_{55}Pd_{55}$ NCs prepared by successive reduction with *L*-ascrobic acid. The STEM images in Figure 5a clearly illustrate again that the prepared catalysts have a uniform size. Since the size of EDS electron beam is 1 nm in diameter, the compositions of different parts of a nanoparticle can be examined independently. The EDS analysis of the randomly chosen NPs (Figure 5b) confirms again that the prepared $Au_{55}Pd_{55}$ NC includes Au, which is in consistence with the ICP results. The reason for the appearance of Pd in EDS may be due to the incomplete coverage of Au atoms on the surface of Pd mother NCs and the diffusion of the incident electron since it is well known that 92 atoms would be needed to cover a $Pd_{55}$ NC based on the knowledge of magic-number cluster. Moreover, the results show that the deposition of Au atoms does not occur homogeneously on the surface of the $Au_{55}Pd_{55}$ NC, and that the deposition of Au atoms seems to result in the formation of Au clusters on the surface by case.

Since the high angle annular dark field (HAADF) method has been used to detect variation in

chemical composition down to a single atom level in proper samples, so it is ideally suitable for composition analysis of the internal structures of nanosized particles. To clarify the morphology and composition profile of the as-prepared Au/Pd SACs at atomic-scale resolution, we secondly studied several independent Au/Pd SAC NCs in Figure 6 and Figure S8 using a probe-corrected (HAADF) STEM. Figure 6a shows the HAADF-STEM images (also known as $Z$-contrast images) of the $Au_3Pd_{55}$ SACs roughly oriented along the [110] zone axis, clearly demonstrating the truncated octahedra morphology. The corresponding fast Fourier-transform (FFT) pattern (in the inset) indicates that the surface of the NC is enclosed with both {111} and {100} facets. It clearly shows the existence of columnar atoms in the $Au_3Pd_{55}$ SACs of ~2.5 nm diameter. A close inspection of the atom arrangement within the individual NC image further reveals that some arrangement possesses orderly alignments, suggesting that they are Pd atoms (dark green dashed rectangle). However, it should be pointed out that the NC in Figure 6a does not form orderly atom alignments around some sites, and clear mismatches are observed in these sites (red circle), which might be caused by the different diameter of Au and Pd atoms (0.276 nm for Pd atom and 0.292 nm for Au atom). The contrast difference caused by the atomic number $Z$ between metal atoms and oxide solids is usually chosen to confirm the presence of single atoms for supported catalysts [14-16]. Nevertheless, even though the atomic number difference between Pd(46) and Au(79) is not small, this method is still hard to be applied to characterize the presence of single Au atoms for the Au/Pd SACs because of the insufficient contrast. It is because that the contrast difference depends not only on the atomic number, $Z,$ of the observed atoms [49-50], but also on the number of total atoms of the observed column.

EELS has been widely used to study the surface composition. In order to confirm the presence of single Au atom on the surface of Pd mother NCs, the EELS measurement was also performed. The

elemental distribution of Pd and Au was obtained by sorting out a specific atom by means of EELS at various locations of an Au/Pd SAC NC. Since the size of the electron beam in EELS is about 0.15 nm ( < Au atom diameter, 0.292 nm), the mapping of a NC by elements can be carried out in detail. Figures 6b and 6c show Au and Pd EELS map (2.86×2.86 nm, 20×20 pixels, and 0.15 nm/pixel), respectively, of an Au/Pd SAC NC accompanied. In the Au EELS map (Figure 6c), the bright areas show the presence of Au atoms. The brighter the area, the more probable it corresponds to Au atom. The corresponding EELS maps of the red circles in Figure 6a are also approximately marked in Figure 6b (the green circles), which suggests that theses atoms in the mismatched sites should be Au atoms, and that Au-single atom distributes in the whole surface of the NC. The presence of Au-single atom on the surface of the mother cluster can be also easily recognized by the composite Au and Pd EELS map shown in Figure 6d (Pd: red; Au: green). However, it should be pointed that the distribution of Au is not completely orderly in the NC, and the Au atoms seem to move in a certain area. This phenomenon can be ascribed to the following two factors. First, the heterogeneous deposition of Au atoms on the surface of Pd mother NCs as shown in Figure 5. Second, the prepared single Au atoms are unstable and easily move during the electron beam irradiation. The similar results were also observed in our previous report of Crown Jewel-Au/Pd NCs [27]. However, the most striking observation is that some single Au atoms do locate at the surface of the Pd mother NC (Figures 6a-6b). Based on the EELS results, the HAADF-STEM images, and the ball schematic sketch shown in Figure 6e, we can conclude that the prepared Au atoms or, at least, parts of them present as single atoms on the surface of the Pd mother NCs.

Using electron tomography to obtain an unambiguous image of the three-dimensional structure of the ultra-small NCs is challenging because these ultra-small NCs are intrinsically structurally unstable and may interact with the incident electron beam [51]. We tried to characterize the surface

composition of a small Au/Pd SAC NC with size less than 2 nm using HAADF-STEM accompanying with EELS (Figure S8). The results show that the small NC may not form a stable structure and easily change its crystalline structure during the HAADF-STEM observation. The geometrical shape of the particle was changed under the irradiation of electron beam. The comparison of the HAADF-STEM image and the EELS Pd map clearly demonstrates this phenomenon. Both the HAADF-STEM image and the EELS Pd map share the same NC but different shapes. Moreover, the widely distributed Au in EELS suggests the breakup of the small Au/Pd SAC NC to atoms under the electron beam irradiation for EELS measurement. Thus, how to get a suitable way to characterize the present Au/Pd SACs is still a problem for us, and further investigations should be carried out in the future. In a word, according to our analysis and interpretation based on the UV-Vis, ICP, TEM, HAADF-STEM and EELS mapping results, it can be concluded that single Au atoms, or at least some of them, formed by the present successive reduction method, are indeed situated on the surface of the Pd mother NC.

### 3.3 Correlation between Structures of Single Au Atoms and Its Catalytic Activity

We evaluated the catalytic activity of the colloidal Au/Pd SACs for aerobic glucose oxidation. The glucose oxidation measurements were performed in water at 60°C at pH of 9.5 under bubbling $O_2$. Generally Au NCs are more active than Pd NCs for this reaction [52], and the active sites can be considered to be Au atoms rather than Pd atoms in the AuPd ally NCs [52, 26]. Thus, the catalytic activity of Au atoms in Au/Pd SACs was evaluated by using equation 1 as mentioned in Experimental section. The initial catalytic activity for the glucose oxidation varies with the elemental composition of the Au/Pd SACs as shown in Figure 7. It clearly indicates that the activities of the Au atoms decrease with the increasing Au content, and that the $Au_{92}Pd_{55}$ NCs with a $Pd_{core}/Au_{shell}$ structure have a low activity of 5,640 mol-glucose·h$^{-1}$·mol-Au$^{-1}$. However, the

maximum catalytic activity of $Au_3Pd_{55}$ SACs is about 142,040 mol-glucose·h$^{-1}$·mol-Au$^{-1}$, which is about 17~40 times higher than those of the monometallic Au NC (even the activity was normalized to the surface atoms) and the Pd NC catalysts, and 5 to 8 times higher than that of the Au/Pd alloy NCs (Figure 8), although all of these NCs possess almost the same particle size. (The TEM images of the Au and Pd monometallic NCs and the Au/Pd alloy NCs are shown in Figure S9.) This result demonstrates that the prepared Au/Pd SACs possess a special structure different from that of the monometallic Pd and Au, and the Au/Pd bimetallic alloy and core/shell NCs. This amazing catalytic activity provides additional indirect proof for the presence of the single Au atoms in the present Au/Pd catalysts. It should be pointed that the catalytic activity of present $Au_3Pd_{55}$ SACs is much lower than that of Crown Jewel-structured Au/Pd SACs (194,980 mol-glucose·h$^{-1}$·mol-Au$^{-1}$) [26], suggesting that most of the reduced Au atoms in present $Au_3Pd_{55}$ SACs are located on the surface of the Pd mother cluster rather than the top sites, and that the structure of the catalyst is crucial for the catalytic activity.

As for the stability of the colloidal Au/Pd SACs, the prepared Au/Pd SACs still held its high catalytic activity for aerobic glucose oxidation even after kept at room temperature for more than 3 months. However, Figure S6 of the titration curve shows that the activity of the $Au_3Pd_{55}$ SAC is high during initial 10 min, and then gradually decreases with the reaction time. This result suggests that the stability of the prepared Au/Pd SACs at 60°C is not good enough. We think that the single Au atoms may move into the inside of the NCs or aggregate each other during the catalysis process because the particle size of the catalyst after glucose oxidation did not change too much in the TEM images, but the single Au atoms in the Pd clusters, on the other hand, had a tendency to move even under the irradiation of electron beam in the HAADF-STEM observation. It is well-known that metallic oxide supported Au catalysts always show a high stability than that of colloidal catalysts.

Hence, we also consider preparing supported Au/Pd SAC catalysts, and the work along these lines is now in progress.

Density functional theory (DFT) has been shown as a powerful tool to provide detailed insight of the interaction between active metal sites and solid supports at the atomic level [53]. To elucidate the nature of the binding of Au single atoms to the Pd NC and the exceptionally high catalytic activity of single Au atoms, theoretical investigations were carried out by using DFT. The $Pd_{55}$ mother NCs with the ideal size of about 1.4 nm can be characterized by a cuboctahedron with eight triangular {111} faces and six square {100} faces. Thus, it is a very interesting question which face the first Au atom prefers to be located at, {111} or {100} face, during the preparation process of the successive reduction. To answer the question, we compared the stabilities of Au atoms located at different facets on the Pd mother NCs by the theoretical calculation with DFT. As shown in Figure 9 and Table S5, our DFT calculations indicate that the most preferable facets for the location of the first reduced Au atoms on the Pd surfaces should be the {111} plane, where each Au atoms is coordinated by three surface Pd atoms. The calculation results show that the adsorption energy of one Au atom on {100} plane is estimated to be 108.5 kJ/mol. In contrast, the adsorption energy on {111} plane is 171.5 kJ/mol. Thus, the adsorption of single Au atoms on {111} plane is concluded to be more stable than that on {100} plane.

We think the high catalytic activity of the Au/Pd SACs should be related to not only the unique geometrical structure but also the electronic properties of the single Au atoms. In order to confirm the electronic properties of the catalytically active Au/Pd SACs, DFT calculations were also carried out to study the electronic states of the single Au atoms in the Au/Pd SACs. DFT calculations of an $Au_8Pd_{55}$ model NPs, where the subscripts stand for the number of atoms in the BNPs, were preformed to assist understanding the electronic states of Pd and Au atoms in the Au/Pd SACs

(Figure 10). The calculations show that Au atoms are indeed negatively charged (-0.197 Mulliken charges), whereas the Pd atoms positively charged, due to the electronic charge transfer from the Pd atoms to the Au ones. This similar electronic charge transfer effect is also observed for Au/Ag [54], Au/Pt/Ag [25] and Pd/Au NCs [26, 55-57]. The possible electronic charge transfer effects in the Au/Pd SACs are illustrated in Figure S10. It is considered that the negatively charged Au atoms acted as catalytic active sites for the glucose oxidation [25-26, 58].

## 4. CONCLUSIONS

Downsizing catalyst nanoparticles to single atoms is very challenging to maximize the utilization efficiency. SACs have been considered a promising avenue to develop future advanced catalysts. For the first time, colloidal Au/Pd SACs with an average diameter of 1.5 nm were prepared by a facile and convenient successive reduction method. This route requires neither annealing process which usually result in the growth and aggregation of the prepared single metal atoms, nor the complex galvanic replacement reaction which was limited to the deposition of more noble element and dissolution of the less noble component.

The activity for glucose oxidation of the colloidal Au/Pd SACs prepared by the successive reduction method is 17-40 times higher than that of the monometallic Au and Pd NCs, and 5 to 8 times higher than that of the Au/Pd alloy NCs with nearly the same particle size. The high catalytic activities of the Au/Pd SACs can be ascribed to the presence of the negatively charged single Au atoms which are formed due to the charge polarization effect induced by the charge transfer from the Pd atoms to the single Au atoms.

Our finding significantly expands the field of single atom catalysts. Although the present study only focused on Au atoms decorating Pd mother clusters used for aerobic glucose oxidation, we

believe that this strategy is also applicable to other kinds of SACs for other catalyzed reactions. We anticipate that the results obtained in this study will provide a clue for the creation of highly efficient novel colloidal Au-containing bi- or multi-metallic catalysts, and that our finding will play an important role to form the basis for exploration of highly efficient single-atom catalysts of the next generation for various applications.

**Supporting information available:** HAADF-STEM images**,** TEM images, UV-Vis spectra, XPS results, preparation conditions and catalytic activities of the CJ-Au/Pd NCs catalyst. An example of the titration curves is also provided. This information is available free of charge via the Internet.

## References

[1] Crespo-Quesada, M.; Yarulin, A.; Jin, M.; Xia, Y.; Kiwi-Minsker, L. Structure sensitivity of alkynol hydrogenation on shape- and size-controlled palladium nanocrystals: Which sites are most active and selective? *J. Am. Chem. Soc.* 2011, 133, 12787–12794.

[2] Herzing, A. A.; Kiely, C. J.; Carley, A. F.; Landon, P.; Hutchings, G. J. Identification of active gold nanoclusters on iron oxide supports for CO oxidation. *Science* 2008, 321, 1331–1335.

[3] Zhang, X. B.; Yan, J. M.; Han, S.; Shioyama, H.; Xu, Q. Magnetically recyclable Fe@Pt core-shell nanoparticles and their use as electrocatalysts for ammonia borane oxidation: The role of crystallinity of the core, *J. Am. Chem. Soc.* 2009, 131, 2778–2779.

[4] Heiz, U.; Sanchez, A.; Abbet, S.; Schneider, W. D. Catalytic oxidation of carbon monoxide on monodispersed platinum clusters: Each atom counts. *J. Am. Chem. Soc.* 1999, 121, 3214–3217.

[5] Lei, Y.; Mehmood, F.; Lee, S.; Greeley, J.; Lee, B.; Seifert, S.; Winans, R. E.; Elam, J. W.; Meyer, R. J.; Redfern, P. C.; Teschner, D.; Schlögl, R.; Pellin, M. J.; Curtiss, L. A.; Vajda, S. Increased silver activity for direct propylene epoxidation via subnanometer size effects. *Science* 2010, 328, 224–228.

[6] Qiao, B.; Liu, L.; Zhang, J.; Deng, Y. Preparation of highly effective ferric hydroxide supported noble metal catalysts for CO oxidations: From gold to palladium. *J. Catal.* 2009, 261, 241–244.

[7] Turner, M.; Golovko, V. B.; Vaughan, O. P. H.; Abdulkin, P.; Berenguer-Murcia, A.; Tikhov, M. S.; Johnson, B. F. G.; Lambert, R. M. Selective oxidation with dioxygen by gold nanoparticle catalysts derived from 55-atom clusters. *Nature* 2008, 454, 981–983.

[8] Kaden, W. E.; Wu, T.; Kunkel, W. A.; Anderson, S. L. Electronic structure controls reactivity of size-selected Pd clusters adsorbed on $TiO_2$ surfaces. *Science* 2009, 326, 826–829.

[9] Chen, M.; Goodman, D.W. The structure of catalytically active gold on titania. *Science* 2004,

306, 252–255.

[10] Haruta, M. Size- and support-dependency in the catalysis of gold. *Catal. Today* 1997, 36, 153–166.

[11] Yang, X. F.; Wang, A. Q.; Qiao, B. T.; Li, J.; Liu, J. Y.; Zhang, T. Single-atom catalysts: A new frontier in heterogeneous catalysis, *Acc. Chem. Res.* 2013, 46(8):1740–1748.

[12] Uzun, A.; Ortalan, V.; Browning, N. D.; Gates, B. C. A site-isolated mononuclear iridium complex catalyst supported on MgO: characterization by spectroscopy and aberration-corrected scanning transmission electron microscopy. *J. Catal.* 2010, 269, 318–328.

[13] Melanie, M. D.; Mina, Y.; Lawrence, F.; Allard, D. R.; Wu, Z. L.; Yang, X. F.; Gabriel, V. G.; Malcolm, S.; Chaitanya, K. N. CO oxidation on supported single Pt atoms: Experimental and ab initio density functional studies of CO interaction with Pt atom on $\theta$-$Al_2O_3$(010) surface, *J. Am. Chem. Soc.* dx.doi.org/10.1021/ja401847c.

[14] Qiao, B.; Wang, A. Q.; Yang, X. F.; Lawrence, F. A.; Jiang, Z.; Cui, Y. T.; Liu, J. Y.; Li, J.; Zhang, T. Single-atom catalysis of CO oxidation using $Pt_1$/FeOx, *Nat. Chem.* 2011, 3: 634-641.

[15] Liu, K.; Wang, A. Q.; Zhang, T. Recent advances in preferential oxidation of CO reaction over platinum group metal catalysts. *ACS Catal.* 2012, 2, 1165-1178.

[16] Lin, J.; Qiao, B. T.; Liu, J. Y.; Huang, Y. Q.; Wang, A. Q.; Li, J.; Zhang, W. S.; Lawrence F. A.; Wang, X. D.; Zhang, T. Design of a highly active Ir/Fe(OH)x catalyst: Versatile application of Pt-Group metals for the preferential oxidation of carbon monoxide, *Angew. Chem. Int. Ed.* 2012, 51, 2920 –2924.

[17] Kwak, J. H.; Kovarik, L.; Szanyi, J. Heterogeneous catalysis on atomically dispersed supported metals: $CO_2$ reduction on multifunctional Pd catalysts. *ACS Catalysis, 2013,* 3(9):2094-2100.

[18] Abbet, S.; Sanchez, A.; Heiz, U.; Schneider, W. D.; Ferrari, A. M.; Pacchioni, G.; RVsch, N.

Cyclotrimerization on supported size-selected $Pd_n$ clusters ($1 \leq n \leq 30$): One atom is enough! *J. Am. Chem. Soc.* 2000, 122, 3453-3457.

[19] Abbet, S.; Heiz, U.; Hakkinen, H.; Landman, U. CO oxidation on a single Pd atom supported on magnesia. *Phys. Rev. Lett.* 2001, 86, 5950-5953.

[20] Sun, S. H.; Zhang, G. X.; Gauquelin, N.; Chen, N.; Zhou, J.; Yang, S. L.; Chen, W. F.; Meng, X. B.; Geng, D. S.; Banis, M. N.; Li, R. Y.; Ye, S. Y.; Knights, S.; Botton, G. A.; Sham, T. K.; Sun, X. L. Single-atom catalysis using Pt/graphene achieved through atomic layer deposition, *Sci. Rep.* 2013, 3(1775):1-9.

[21] Zhang, R. Q.; Lee, T. H.; Yu, B. D.; Stampfl, C.; Soon, A. The role of titaniumnitride supports for single-atom platinum-based catalysts in fuel cell technology. *Phys. Chem. Chem. Phys.* 2012, 14, 16552–16557.

[22] Kyriakou, G.; Boucher, M. B.; Jewell, A. D.; Lewis, E. A.; Lawton, T. J.; Baber, A. E.; Tierney, H. L.; Flytzani-Stephanopoulos, M.; Sykes, E. C. Isolated metal atom geometries as a strategy for selective heterogeneous hydrogenations. *Science* 2012, 335, 1209–1212.

[23] Uzun, A., Ortalan, V., Hao, Y., Browning, N. D. & Gates, B. C. Nanoclusters of gold on a high-area support: almost uniform nanoclusters imaged by scanning transmission electron microscopy. *ACS Nano* 2009, 3, 3691–3695.

[24] Jirkovsky, J. S.; Panas, I.; Ahlberg, E.; Halasa, M.; Romani, S.; Schiffrin, D. J. Single atom hot-spots at Au-Pd nanoalloys for electrocatalytic $H_2O_2$ production. *J. Am. Chem. Soc.* 2011, 133, 19432–19441.

[25] Zhang, H. J.; Okumura, M.; Toshima, N. Stable Dispersions of PVP-Protected Au/Pt/Ag Trimetallic Nanoparticles as Highly Active Colloidal Catalysts for Aerobic Glucose Oxidation. *J. Phys. Chem. C* 2011, 115 (30), 14883–14891.

[26] Zhang, H. J.; Watanabe, T.; Okumura, M.; Haruta, M.; Toshima, N. Crown Jewel catalyst: How neighboring atoms affect the catalytic activity of top Au atoms? *J. Catal.* 2013, 305, 7–18.

[27] Zhang, H. J.; Watanabe, T.; Okumura, M.; Haruta, M.; Toshima, N. Catalytically highly active top gold atom on palladium nanocluster, *Nat. Mater.* 2012, 11, 49-52.

[28] Teng, X. W.; Wang, Q.; Liu, P.; Han, W. Q.; Frenkel, A. I.; Wen, W. ; Marinkovic, N.; Hanson, J. C.; Rodriguez, J. A. Formation of Pd/Au nanostructures from Pd nanowire via galvanic replacement reaction. *J. Am. Chem. Soc.* 2008, 130, 1093-1101.

[29] Edwards, J. K.; Solsona, B.; Ntainjua, N, E.; Carley, A. F.; Herzing, A. A.; Kiely, C. J.; Hutchings, G. J. Switching-Off Hydrogen Peroxide Hydrogenation In The Direct Synthesis Process. *Science* 2009, 323, 1037-1041.

[30] Landon, P.; Collier, P. J.; Papworth, A. J.; Kiely, C. J.; Hutchings, G. J. Direct formation of hydrogen peroxide from $H_2/O_2$ using a gold catalyst. *Chem. Commun.* 2002, 5(18), 2058-2059.

[31] Enache, D. I.; Edwards, J. K.; Landon, P.; Solsona-Espriu, B.;   Carley, A. F.; Herzing, A. A.; Watanabe, M.; Kiely, C. J.; Knight, D. W. ; Hutchings, G. J. Solvent-free oxidation of primary alcohols to aldehydes using Au-Pd/$TiO_2$ catalysts. *Science* 2006, 311, 362-365.

[32] Venezia, A. M.; Liotta, L. F.; Pantaleo, G.; La Parola, V.; Deganello, G.; Beck, A.; Koppany, Z.; Frey, K.; Horvath, D.; Guczi, L. Activity of $SiO_2$ supported gold-palladium catalysts in CO oxidation. *Appl. Catal. A* 2003, 251, 359-368.

[33] Bonarowska, M.; Malinowski, A.; Juszczyk, W.; Karpinski, Z. Hydrodechlorination of $CCl_2F_2$ (CFC-12) over silica-supported palladium-gold catalysts. *Appl. Catal. B* 2001, 30, 187-193.

[34] Mizukoshi, Y.; Fujimoto, T.; Nagata, Y.; Oshima, R.; Maeda, Y. Characterization and catalytic activity of core-shell structured gold/palladium bimetallic nanoparticles synthesized by the sonochemical method. *J. Phys. Chem. B* 2000, 104, 6028-6032.

[35] Venezia, A. M.; La Parola, V.; Deganello, G.; Pawelec, B.; Fierro, J. L. G. Synergetic effect of gold in Au/Pd catalysts during hydrodesulfurization reactions of model compounds. *J. Catal.* 2003, *215*, 317-325.

[36] Toshima, N.; Kanemaru, M.; Shiraishi, Y; Koga, Y. Spontaneous formation of core/shell bimetallic nanoparticles: a calorimetric study. *J. Phys. Chem. B* 2005, 109, 16326-16331.

[37] Jongh, L. J.; Baak, J.; Brom, H. B.; Putten, D. V. D. in: P. Jena, S. N. Khanna, B. K. Rao (Eds.), Physics and chemistry of fine systems: From clusters to crystals, Kluwer, Dordrecht, 1992, vol. II, p. 839.

[38] Schmid, G. *In metal clusters in chemistry*: P. Braunstein, L. A. Oro, P. R. Raithby, Eds.; Wiely-VCH: Weinheim, 1999, 3, 1325.

[39] Lee, A. F.; Baddeley, C. J.; Hardacre, C.; Ormerod, R. M.; Lambert, R. M.; Schmid, G.; West, H. Structural and catalytic properties of novel Au/Pd bimetallic colloid particles - EXAFS, XRD and acetylene coupling. *J. Phys. Chem.* 1995, 99, 6096-6102.

[40] Nutt, M. O.; Hughes J. B.; Wong, M. S.; Nutt, M. O.; Hughes, J. B.; Wong, M. S. Designing Pd-on-Au bimetallic nanoparticle catalysts for trichloroethene hydrodechlorination. *Environ. Sci. Technol.* 2005, 39, 1346-1353.

[41] Wang, Y.;  Toshima, N. Preparation of Pd-Pt bimetallic colloids with controllable core/shell structures. *J. Phys. Chem. B* 1997, 101, 5301-5306.

[42] Shiraishi, Y.; Ikenaga, D.; Toshima, N. Preparation and catalysis of inverted core/shell structured Pd/Au bimetallic nanoparticles. Aust. *J. Chem.* 2003, 56, 1025-1029.

[43] Scott, R. W. J.; Wilson, O. M.; Oh, S. K.; Kenik E. A.; Crooks, R. M. Bimetallic palladium-gold dendrimer-encapsulated catalysts. *J. Am. Chem. Soc.* 2004, 126, 15583-155591.

[44] Lim, B.; Kobayashi, H.; Yu, T.; Wang, J.; Kim, M. J.; Li, Z. -Y.; Rycenga, M.; Xia, Y.

Synthesis of Pd−Au bimetallic nanocrystals via controlled overgrowth. *J. Am. Chem. Soc*. 2010, 132, 2506-2507.

[45] Kan, C. X.; Cai, W. P.; Li, C. C.; Zhang, L. D.; Hofmeister, H. Ultrasonic synthesis and optical properties of Au/Pd bimetallic nanoparticles in ethylene glycol. *J. Phys. D* 2003, 36, 1609-1614.

[46] Lim, B.; Wang, J.; Camargo, P. H. C.; Jiang, M.; Kim, M. J.; Xia, Y. Facile synthesis of bimetallic nanoplates consisting of Pd cores and Pt shells through seeded epitaxial growth. *Nano Lett.* 2008, 8, 2535-2540.

[47] Fan, F. R.; Liu, D. Y.; Wu, Y. F.; Duan, S.; Xie, Z. X.; Jiang, Z. Y.; Tian, Z. Q. Epitaxial growth of heterogeneous metal nanocrystals: from gold nano-octahedra to palladium and silver nanocubes. *J. Am. Chem. Soc.* 2008, 130, 6949.

[48] Ferrer, D.; Torres-Castro, A.; Gao, X.; Sepffllveda-Guzmn, S. Three-layer core/shell structure in Au-Pd bimetallic nanoparticles. *Nano Lett.* 2007, 7, 1701-1705.

[49] Li, Z. Y.; Yuan, J.; Chen Y.; Palmer, R. E.; Wilcoxon, J. P. Direct imaging of core-shell structure in silver-gold bimetallic nanoparticles, *Appl. Phys. Lett.* 2005, 87, 243103.

[50] Habas, S. E.; Lee, H. J.; Radmilovic, V.; Somorjai, G. A.; Yang, P. D. Shaping Binary Metal Nanocrystals Through Epitaxial Seeded Growth. *Nat. Mater.* 2007, 6, 692.

[51] Li, Z. Y.; Young, N. P.; DiVece, M.; Palomba, S.; Palmer, R. E.; Bleloch, A. L.; Curley, B. C.; Johnston, R. L.; Jiang, J.; Yuan, J. *Nature* 2007, *451*, 46.

[52] Comotti, M.; Della Pina, C.; Matarrese, R.; Rossi, M. The Catalytic Activity of "Naked" Gold Particles, *Angew. Chem. Int. Ed*. 2004, 43, 5812.

[53] Zhang, J.; Alexandrova, A. N. The golden crown: A single Au atom that boosts the CO oxidation catalyzed by a palladium cluster on titania surfaces, *J. Phys. Chem. Lett.* 2013, 4, 2250−2255.

[54] Chaki, N. K.; Tsunoyama, H.; Negishi, Y.; Sakurai, H.; Tsukuda, T. *J. Phys. Chem. C.* 2007, 111: 4885-4888.

[55] Yuan, X.; Sun, G.; Asakura, H.; Tanaka, T.; Chen, X.; Yuan, Y.; Laurenczy, G.; Kou, Y.; Dyson, P. J.; Yan, N. Development of palladium surface-enriched heteronuclear Au-Pd nanoparticle dehalogenation catalysts in an ionic liquid, *Chemistry - A European Journal*, 2013, 19(4): 1227-1234.

[56] Bruma, A.; Negreiros, F.R.; Xie, S.; Tsukuda, T.; Johnston, R.L.; Fortunelli, A.; Li, Z.Y. Direct atomic imaging and density functional theory study of the $Au_{24}Pd_1$ cluster catalyst, *Nanoscale*, 2013, 5(20): 9620-9625.

[57] Zhou, Y.; Itoh, H.; Uemura, T.; Naka, K.; Chujo, Y., Synthesis of novel stable nanometer-sized metal (M = Pd, Au, Pt) colloids protected by a π-conjugated polymer, *Langmuir*, 2002, (18)1: 277-283.

[58] Tokonami, S.; Morita, N.; Takasaki, K.; Toshima, N. Novel Synthesis, Structure, and Oxidation Catalysis of Ag/Au Bimetallic Nanoparticles, *J. Phys. Chem. C*, 2010, *114,* 10336-10341.

**Figure captions**

*Figure 1.* Schematic illustration for the deposition of single Au atom on Pd mother clusters by successive reduction method using L-ascrobic acid as reductant.

*Figure 2.* UV-Vis spectra of colloidal dispersions of Au/Pd SACs with various compositions prepared by *L*-ascrobic acid reduction (Preparation conditions of Pd: 90°C/15min; Reaction conditions of Au/Pd BNCs: 95°C/15min).

*Figure 3.* TEM micrographs of Au/Pd SACs with various compositions prepared by *L*-ascrobic acid reduction (reaction conditions: 95°C/15min).

*Figure 4.* Composition data of Au content in Au/Pd SACs derived from ICP analysis (The plot shows the relationship between the Au% from the synthetic feed and Au % in the final NCs, the dotted line shows the theoretical contents of Au.).

*Figure 5.* HR-STEM (a) image, and EDS results (b) of the final $Au_{55}Pd_{55}$ catalysts prepared by *L*-ascrobic acid reduction.

*Figure 6.* HAADF-STEM image and EELS mapping of $Au_3Pd_{55}$ Au/Pd SACs. (a) HAADF-STEM image of a single $Au_3Pd_{55}$ SACs, (b) and (c) EELS element map of Au and Pd shows the segregated distribution of Pd and Au atoms in a NC, **(c)** Composite EELS map of a HAADF image showing mainly Pd (red) and distribution of Au (green) in a NC, **(d)** Ball schematic sketch shows the NC model along the [110] zone axis of $Au_8Pd_{55}$ SACs.

*Figure 7.* Catalytic activity of Au/Pd SACs for glucose oxidation with various compositions prepared by *L*-ascrobic acid reduction.

*Figure 8.* Comparison of the catalytic activity of Au/Pd SACs, Au, Pd, and Au/Pd alloy NCs for aerobic glucose oxidation. (Schematic inserts and numbers shown at the top of each bar indicate the

structure models and the average particle sizes, respectively, of the NCs ; Au*, the activity was

normalized by the number of surface Au atoms in NCs; Pd*, the activity of the mother clusters

which was normalized by the number of surface Pd atoms with a value of 3, 500

mol-glucose·h$^{-1}$·mol-surface Pd$^{-1}$.)

**Figure 9.** Calculated adsorption energy of single Au atoms anchored to {100} and {111} face by

DFT.

**Figure 10.** DFT calculations of electronic structure of (a) core/shell-structured Au/Pd NCs and (b)

Au/Pd SACs (Yellow: Au atoms; Dark blue: Pd atoms).

{100}

{111}

Pd$_{55}$, 1.4 nm

+ Au$^{3+}$

90°C, N$_2$

L-ascrobic acid

◯ Pd atoms

◯ Au atoms

Au atoms embedded
on Pd NCs

**Figure 1**

**Figure 2**

(a) SA-1, $Au_3Pd_{55}$            (b) SA-2, $Au_6Pd_{55}$

(c) SA-3, $Au_{14}Pd_{55}$           (d) SA-4, $Au_{28}Pd_{55}$

(e) SA-5, $Au_{55}Pd_{55}$           (f) SA-6, $Au_{92}Pd_{55}$
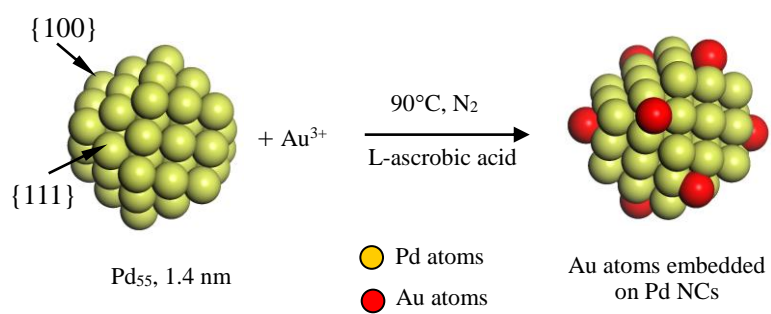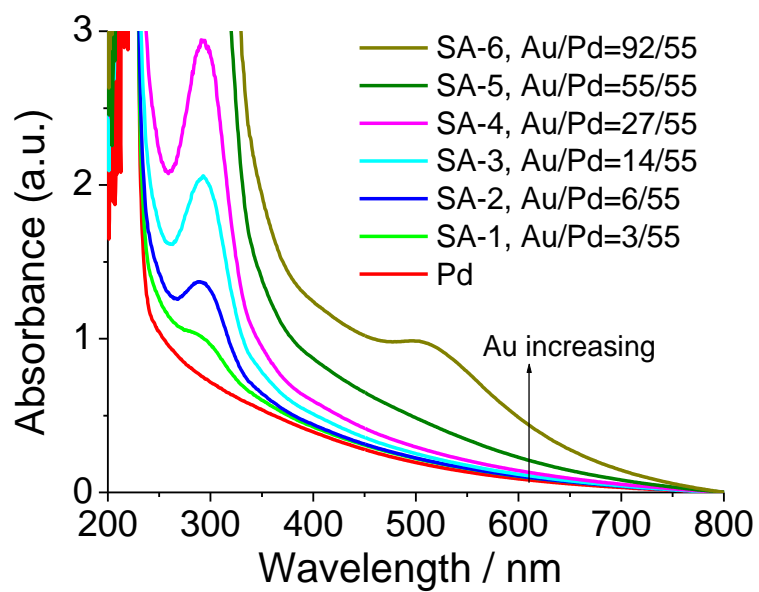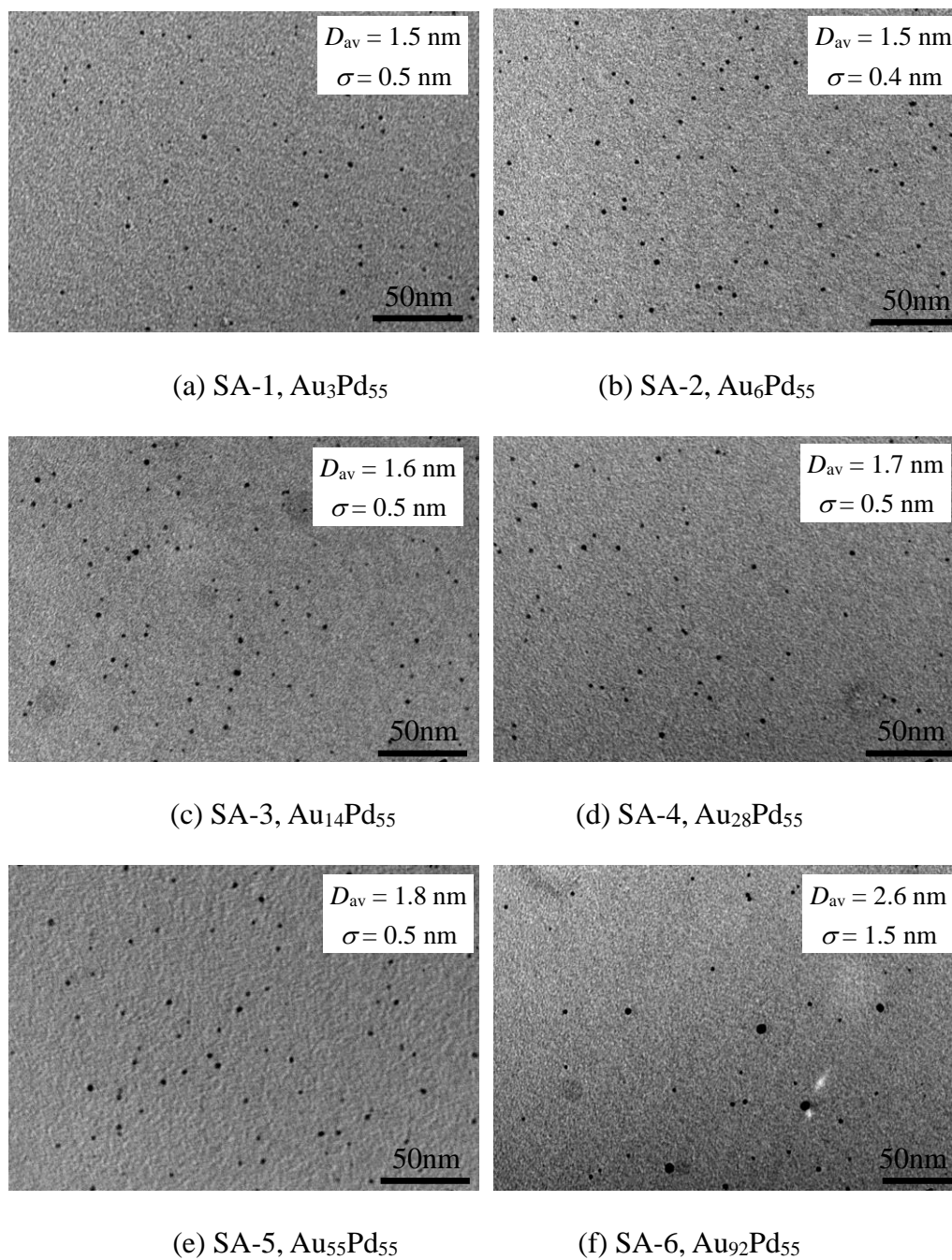
**Figure 3**

33
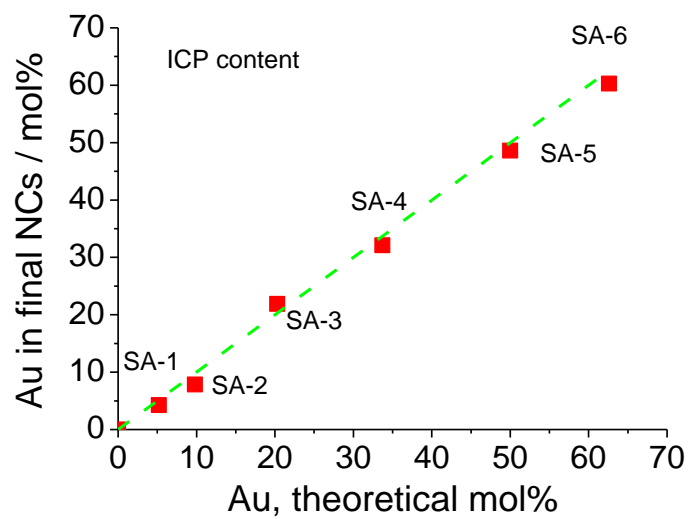
*Figure 4*
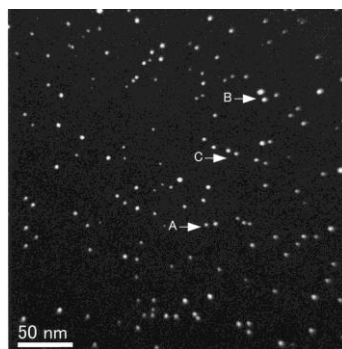
(a) STEM of SA-5



| Particles | spot | Chemical compositions, atom% | |
|---|---|---|---|
| | | Pd | Au |
| Particle 1 | center | 82 | 18 |
| | edge | 53 | 47 |
| Particle 2 | center | 60 | 40 |
| | edge | 64 | 36 |
| Particle 3 | center | 82 | 18 |
| | edge | 38 | 62 |
| Particle 4 | center | 59 | 41 |
| | edge | 69 | 31 |
| Particle 5 | center | 55 | 45 |
| | edge | 35 | 65 |
| Particle 6 | center | 83 | 17 |
| | edge | 77 | 23 |
| Mean contents | center | 70 | 30 |
| | edge | 56 | 44 |

(b) STEM-EDS of SA-5

**Figure 5**
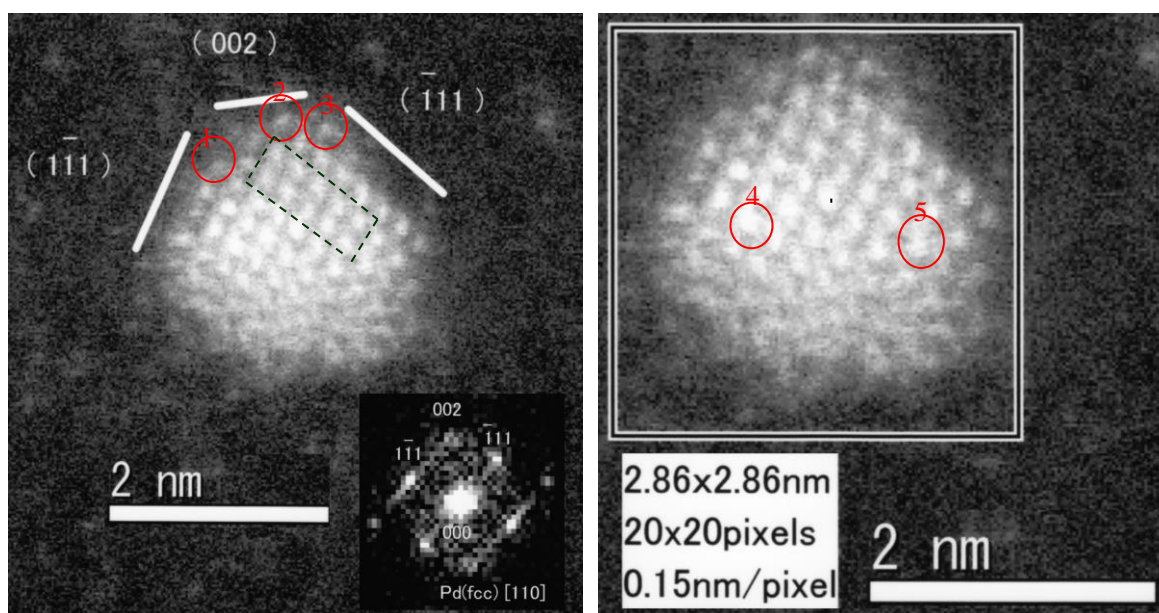
(a) HAADF-STEM of SA-1
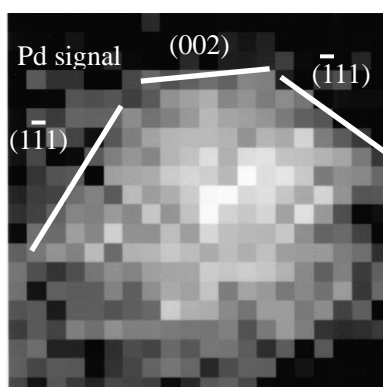


(b) EELS of Pd
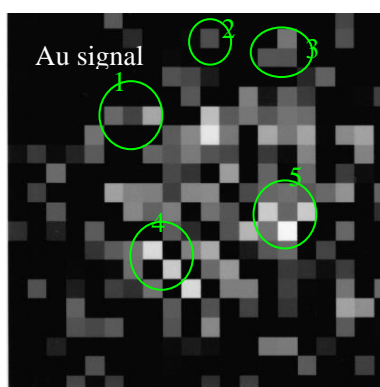


(c) EELS of Au
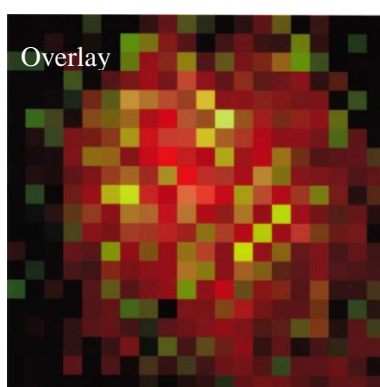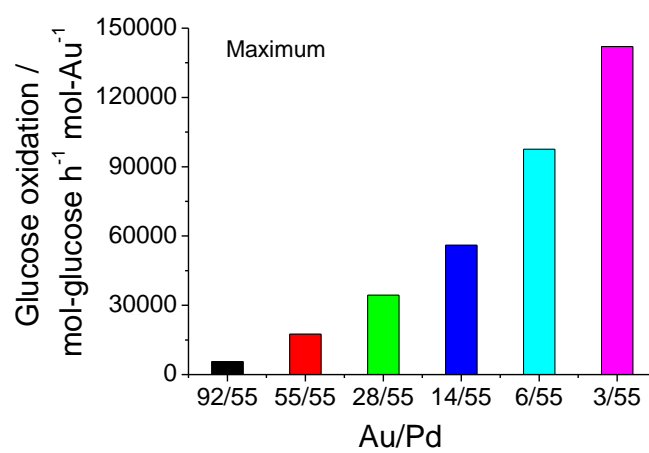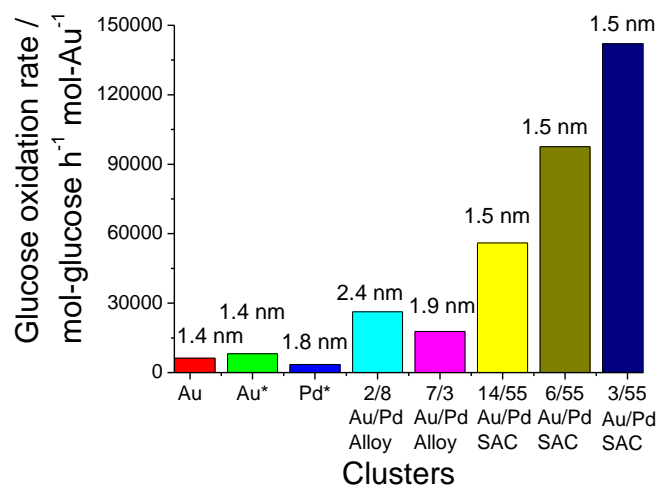


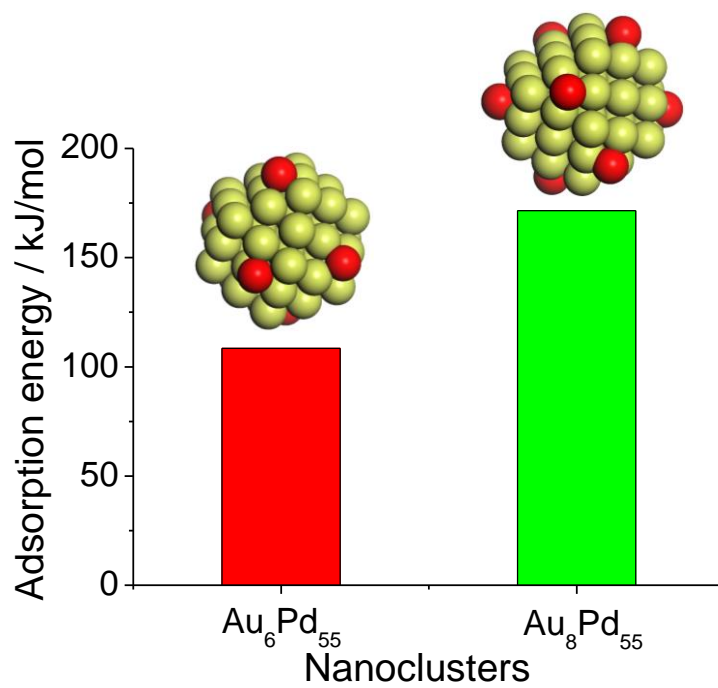(d) Composite EELS mapping
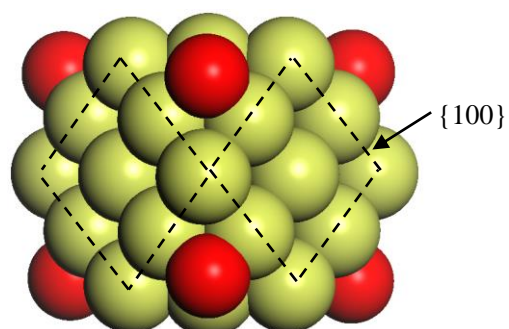


(e) Ball schematic sketch

**Figure 6**

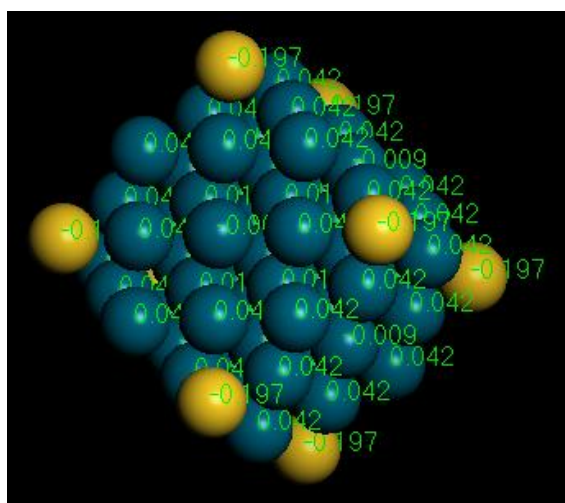**Figure 7**

**Figure 8**

**Figure 9**

**Figure 10**